




## Peak-Luminosity/Decline-Rate Relationship for Tidal Disruption Events

JASON T. HINKLE <sup>1</sup>, THOMAS W.-S. HOLOIEN <sup>2</sup>, BENJAMIN. J. SHAPPEE <sup>1</sup>, KATIE AUCHETTL<sup>3,4</sup>,  
CHRISTOPHER S. KOCHANÉK,<sup>5,6</sup> K. Z. STANEK,<sup>5,6</sup> ANNA V. PAYNE,<sup>1,\*</sup> AND TODD A. THOMPSON<sup>5,6</sup>

<sup>1</sup>*Institute for Astronomy, University of Hawai'i, 2680 Woodlawn Dr., Honolulu, HI 96822, USA*

<sup>2</sup>*The Observatories of the Carnegie Institution for Science, 813 Santa Barbara St., Pasadena, CA 91101, USA*

<sup>3</sup>*DARK, Niels Bohr Institute, University of Copenhagen, Lyngbyvej 2, 2100 Copenhagen, Denmark*

<sup>4</sup>*Department of Astronomy and Astrophysics, University of California, Santa Cruz, CA 95064, USA*

<sup>5</sup>*Department of Astronomy, The Ohio State University, 140 West 18th Avenue, Columbus, OH 43210, USA*

<sup>6</sup>*Center for Cosmology and Astroparticle Physics, The Ohio State University, 191 W. Woodruff Avenue, Columbus, OH 43210, USA*

Submitted to ApJL

### ABSTRACT

We compare the luminosity, radius, and temperature evolution of the UV/optical blackbodies for fifteen well-observed tidal disruption events (TDEs), eight of which were discovered by the All-Sky Automated Survey for Supernovae (ASAS-SN). We find that the blackbody radii generally increase prior to peak and slowly decline at late times. The blackbody temperature evolution is generally flat, with a few objects showing small-scale variations. The bolometric UV/optical luminosities generally evolve smoothly and flatten out at late times. Finally, we find an apparent correlation between the peak luminosity and the decline-rate of TDEs. This relationship is strongest when comparing the peak luminosity to its decline over 40 days. A linear fit yields  $\log_{10}(L_{\text{peak}}) = (44.1^{+0.1}_{-0.1}) + (1.1^{+0.3}_{-0.3})(\Delta L_{40} + 0.5)$  in cgs, where  $\Delta L_{40} = \log_{10}(L_{40}) - \log_{10}(L_{\text{peak}}) = \log_{10}(L_{40}/L_{\text{peak}})$ .

*Keywords:* Black hole physics (159) — Supermassive black holes (1663) — Tidal disruption (1696) — Transient sources (1851)

### 1. INTRODUCTION

A tidal disruption event (TDE) occurs when a star passes inside the tidal radius of a supermassive black hole (SMBH). The self-gravity of the star is overwhelmed by tidal forces and the star is ripped apart. This results in a luminous accretion flare (e.g., Rees 1988; Evans & Kochanek 1989; Phinney 1989; Ulmer 1999), with a blackbody temperature on the order of  $\sim 10^5$  K (e.g., Lacy et al. 1982; Rees 1988; Evans & Kochanek 1989; Phinney 1989).

The characteristics of the observed emission from TDEs may depend on a large number of physical parameters. These include the star's impact parameter (e.g., Guillochon & Ramirez-Ruiz 2013, 2015), stellar properties such as mass (e.g., Gallegos-Garcia et al.

2018; Mockler et al. 2019), age (e.g., Gallegos-Garcia et al. 2018), spin (e.g., Golightly et al. 2019), composition (e.g., Kochanek 2016a), evolutionary stage (e.g., MacLeod et al. 2012), stellar demographics (e.g., Kochanek 2016b), the fraction of accreted stellar material (e.g., Metzger & Stone 2016; Coughlin & Nixon 2019); the geometry of accretion (e.g., Kochanek 1994; Guillochon & Ramirez-Ruiz 2015; Dai et al. 2018); and the black hole mass and spin (e.g., Ulmer 1999; Graham et al. 2001; Mockler et al. 2019).

Despite the large number of possibly relevant physical parameters, the UV/optical spectral energy distributions of TDEs are well-fit as blackbodies (e.g., Holoien et al. 2014, 2016a,b; Brown et al. 2016; Hung et al. 2017; Holoien et al. 2018, 2019a; Leloudas et al. 2019; van Velzen et al. 2020). Generally, the effective radii increase until peak before declining monotonically. The temperature evolution is occasionally more variable, but temperatures generally remain relatively constant, sometimes increasing at late times (e.g. Holoien et al. 2019b; van Velzen et al. 2020). The luminosity evolution is gen-

Corresponding author: Jason T. Hinkle  
jhinkle6@hawaii.edu

\* NASA Fellowship Activity Fellow

erally smooth, with only a handful of sources showing spikes or rebrightening episodes. TDE models such as those of Dai et al. (2018), Lu & Bonnerot (2019), and Ryu et al. (2020) may help to explain the wide range in observed properties and variations in blackbody evolution.

Pre-peak detections of TDEs are important to understanding the evolution of the UV/optical blackbody component before and after peak emission. However, TDEs are rare, with an expected frequency between  $10^{-4}$  and  $10^{-5}$  yr $^{-1}$  per galaxy (e.g., van Velzen & Farrar 2014; Holoien et al. 2016a) and the discovery of TDEs before maximum brightness is challenging. Fortunately, current transient surveys like the All-Sky Automated Survey for Supernovae (ASAS-SN; Shappee et al. 2014; Kochanek et al. 2017), the Asteroid Terrestrial Impact Last Alert System (ATLAS; Tonry et al. 2018), the Panoramic Survey Telescope and Rapid Response System (Pan-STARRS; Chambers et al. 2016), and the Zwicky Transient Facility (ZTF; Bellm et al. 2019) are discovering many more TDEs, with an increasing number being discovered prior to their peak (e.g., Holoien et al. 2019b,a; Leloudas et al. 2019; Wevers et al. 2019; van Velzen et al. 2020, Hinkle et al. in prep.; Payne et al. in prep.).

In this paper, we note a correlation between the peak luminosity of a TDE and its decline-rate. In Section 2, we define the sample and our blackbody models of the UV/optical emission. In Section 3, we discuss the peak-luminosity/decline-rate relationship. Finally, in Section 4 we summarize the main results of our analysis. Throughout our analysis we assume a cosmology of  $H_0 = 69.6$  km s $^{-1}$  Mpc $^{-1}$ ,  $\Omega_M = 0.29$ , and  $\Omega_\Lambda = 0.71$ .

## 2. SAMPLE AND MODELS

Because UV-optical TDEs have observed temperatures of 20,000 to 50,000 K, we require UV observations to accurately determine a blackbody fit. To be included in our sample, a TDE must have been observed by the Neil Gehrels Swift Gamma-ray Burst Mission (*Swift*; Gehrels et al. 2004) satellite, using the UltraViolet and Optical Telescope (UVOT; Roming et al. 2005) for at least fifteen epochs with photometric observations in all of the *Swift* UV filters: *UVW1* (2600 Å), *UVM2* (2246 Å) and *UVW2* (1928 Å) (Poole et al. 2008). The fifteen TDEs satisfying these criteria are listed in Table 1.

We divided the sources into three classes depending on how well the peak luminosity could be characterized. Class “A” sources have *Swift* photometry spanning the peak bolometric luminosity. Class “B” sources have ground-based data spanning the peak and *Swift* observations within ten days of the peak to estimate a bolomet-

ric correction for the ground-based data at peak. Class “C” sources were either not observed until after peak or lacked *Swift* observations within ten days of peak so that bolometric corrections at peak are less reliable. We include the class of each source in Table 1 along with the spectroscopic classifications introduced by van Velzen et al. (2020). Of the 15 TDEs, all but one either show evidence for Bowen fluorescence emission (TDE-Bowen) or strong H lines (TDE-H), with only one showing strong He (relative to H) lines (TDE-He).

We used Markov Chain Monte Carlo (MCMC) methods to fit a blackbody model to each epoch of *Swift* observations for the TDEs in our sample. To keep our fits relatively unconstrained, we ran each of our blackbody fits with flat temperature priors of  $10000 \text{ K} \leq T \leq 55000 \text{ K}$ . In Figure 1, we compare the evolution of the blackbody parameters of all the TDEs in our sample. For this figure, we smooth the lines for luminosity, radius, and temperature evolution for each TDE, by linearly interpolating to a time-series with the same length as the original coverage, but with one-third the number of points. This allows us to compare general trends, without being overly sensitive to short-timescale variations or individual epochs of poor data quality. We use the time in rest-frame days relative to the peak luminosity for the objects where we could constrain the time of peak light (ASASSN-19dj, ASASSN-19bt, ASASSN-18pg, ASASSN-18ul, PS18kh, iPTF16-fnl, Gaia19bpt, and ZTF19abzrhgq) and in rest-frame days relative to discovery for those where we could not (ASASSN-15oi, ASASSN-14ae, ASASSN-14li, iPTF16axa, ASASSN-18zj, ATLAS18way, and ZTF19aapreis).

In general, the blackbody radii increase before peak light, reaching a maximum radius near the peak or soon thereafter. After the blackbody radius peaks, there is a generally monotonic decline in size. For the TDEs with well-sampled late-time evolution (ASASSN-19dj, ASASSN-18pg, ATLAS18way, ASASSN-15oi, and ASASSN-14li), the blackbody radii continue to slowly decrease. Like van Velzen et al. (2020), we find that the TDE-Bowen objects have smaller effective blackbody radii than the TDE-H objects.

For most of the TDEs in our sample, the blackbody temperatures stay constant given the uncertainties as they evolve. In some cases, such as ASASSN-19dj and ASASSN-18pg, there is some evolution in temperature over the first  $\sim 50$  days, but the general trend is flat. There are some exceptions, with ASASSN-19bt decreasing in temperature over time and ASASSN-15oi and PS18kh both increasing in temperature. The TDE-Bowen objects are hotter than the TDE-H objects, in agreement with van Velzen et al. (2020).

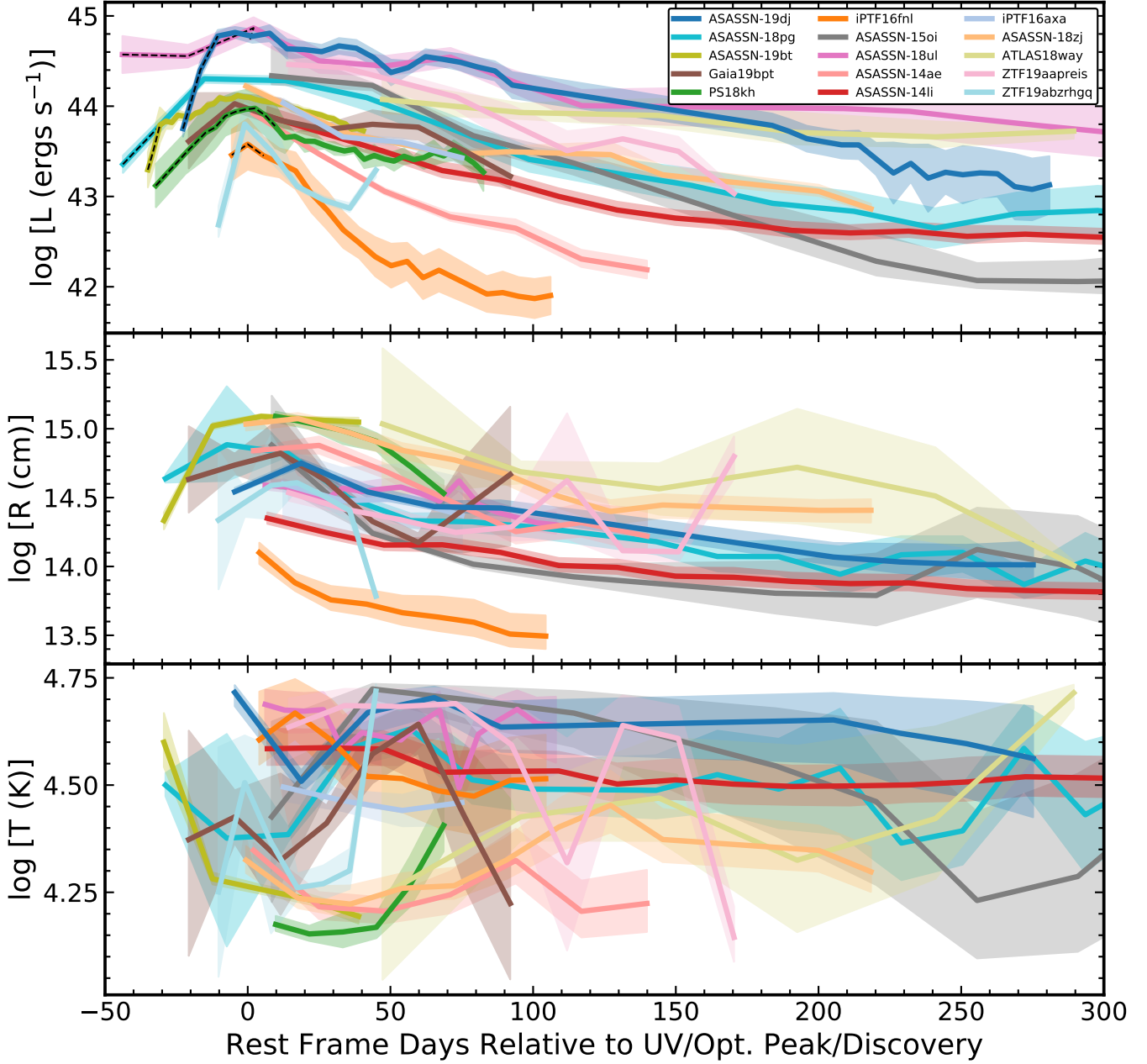


**Figure 1.** Evolution of the UV/optical blackbody luminosity (top panel), effective radius (middle panel), and temperature (bottom panel) for the TDEs ASASSN-19dj (blue line), ASASSN-18pg (cyan line), ASASSN-19bt (olive line), Gaia19bpt (brown line), PS18kh (green line), iPTF16fnl (orange line), ASASSN-15oi (gray line), ASASSN-18ul (pink line), ASASSN-14ae (salmon line), ASASSN-14li (red line), iPTF16axa (light-purple line), ASASSN-18zj (light-orange line), ATLAS18way (light-olive line), ZTF19aapreis (light-pink line), and ZTF19abzrhgq (light-blue line). The lines are smoothed over the individual epochs by linearly interpolating to a time-series with the same length as the original coverage, but with one-third the number of points. Time is in rest-frame days relative to the peak luminosity for the class “A” and “B” objects, where we could constrain the time of peak light (ASASSN-19dj, ASASSN-19bt, ASASSN-18pg, ASASSN-18ul, PS18kh, iPTF16-fnl, Gaia19bpt, and ZTF19abzrhgq) and in rest-frame days relative to discovery for the class “C” objects, where we could not (ASASSN-15oi, ASASSN-14ae, ASASSN-14li, iPTF16axa, ASASSN-18zj, ATLAS18way, and ZTF19aapreis). Dashed lines (for ASASSN-19bt, ASASSN-18pg, ASASSN-18ul, PS18kh, iPTF16fnl, and ASASSN-19dj) indicate where data has been bolometrically corrected using the ASAS-SN or PTF *g*-band light curve assuming the temperature from the first *Swift* epoch.

**Table 1.** Sample of TDEs

Object	Class	Spectral Type	References
ASASSN-19dj	A	TDE-Bowen	<a href="#">Liu et al. (2019)</a> , <a href="#">van Velzen et al. (2020)</a> , Hinkle et al. in prep.
ASASSN-18pg	A	TDE-Bowen	<a href="#">Leloudas et al. (2019)</a> , Holoien et al. in prep.
ASASSN-19bt	A	TDE-H	<a href="#">Holoien et al. (2019a)</a>
Gaia-19bpt	A	TDE-H	<a href="#">Gezari et al. (2019)</a>
ZTF19abzrhgq	A	TDE-Bowen	<a href="#">van Velzen et al. (2020)</a>
ASASSN-18ul	B	TDE-Bowen	<a href="#">Wevers et al. (2019)</a> , Payne et al. in prep.
PS18kh	B	TDE-H	<a href="#">Holoien et al. (2018)</a>
iPTF16fml	B	TDE-Bowen	<a href="#">Brown et al. (2018)</a>
ASASSN-15oi	C	TDE-He	<a href="#">Holoien et al. (2016a)</a>
ASASSN-14ae	C	TDE-H	<a href="#">Holoien et al. (2014)</a>
ASASSN-14li	C	TDE-Bowen	<a href="#">Holoien et al. (2016b)</a>
iPTF16axa	C	TDE-Bowen	<a href="#">Hung et al. (2017)</a>
ASASSN-18zj	C	TDE-H	<a href="#">Dong et al. (2018)</a>
ATLAS18way	C	TDE-H	<a href="#">van Velzen et al. (2018)</a>
ZTF19aapreis	C	TDE-Bowen	<a href="#">van Velzen et al. (2020)</a>

NOTE—The fifteen TDEs studied in this paper. Class “A” means that there is *Swift* data prior to the peak bolometric luminosity, class “B” means that the TDE was observed with *Swift* within 10 days of peak combined with ground-based photometry of the peak, and class “C” means the TDE was either not observed until after peak or lacked *Swift* observations within ten days of peak so that bolometric corrections at peak are less reliable. The spectral types are taken from [van Velzen et al. \(2020\)](#).

The bolometric UV/optical luminosities of the TDEs in our sample rise to peak at varying rates, and decrease roughly monotonically thereafter. The luminosity evolution of most of the objects is smooth, but some TDEs like ASASSN-18ul, PS18kh, and ASASSN-19bt have features such as luminosity spikes or re-brightening episodes. Multiple peaks in the UV/optical luminosity could either be due to shocks caused by collisions in the debris stream (e.g., Gezari et al. 2017) or caused by reprocessing of X-ray emission from an accretion disk (e.g., Wevers et al. 2019; Leloudas et al. 2019). The TDE-Bowen objects, with the exceptions of iPTF16fnl and ZTF19abzrhgq, are generally more luminous than the TDE-H objects, although the differences in luminosity are smaller than for the radii and temperatures.

### 3. PEAK-LUMINOSITY/DECLINE-RATE RELATIONSHIP

In Figure 1, the most luminous TDEs appear to have flatter slopes near peak, and thus decay more slowly than the less luminous TDEs. This is reminiscent of the Phillips relation for Type Ia supernovae (SNe Ia; Phillips 1993), except that for TDEs it is the bolometric evolution rather than the evolution in individual photometric passbands. This suggested trying to define a similar relationship for TDEs.

To determine the peak luminosity ( $L_{\text{peak}}$ ) for the class “A” and “B” TDEs with ground-based observations prior to peak, we first bolometrically corrected the ground-based  $g$ -band data using a linear interpolation between the *Swift* blackbody fits before and after each  $g$  observation to calculate a bolometric correction. We used the first *Swift* epoch to define the bolometric correction for all prior epochs of ground-based observation. We then fitted a quadratic to the combined, bolometrically-corrected  $g$ -band and *Swift* data to find the peak date and luminosity as well as the associated uncertainties. For the two ZTF objects, we did not perform bolometric corrections because there was not enough  $g$ -band data. For class “C” objects, we simply used the maximum luminosity as  $L_{\text{peak}}$ , with the uncertainty on that estimate as the uncertainty on the peak luminosity. We incorporated uncertainties in distance into the uncertainties on peak luminosity. These come from both uncertainties in the value of the Hubble constant and the spread in observed peculiar velocities. We took the sum of the statistical and systematic errors from Freedman et al. (2019) and assume an error of  $2.5 \text{ km s}^{-1} \text{ Mpc}^{-1}$  on  $H_0$ . From the observed distribution of peculiar velocities in the nearby Universe, we assume a representative spread of  $500 \text{ km s}^{-1}$  (e.g., Tully et al. 2016).

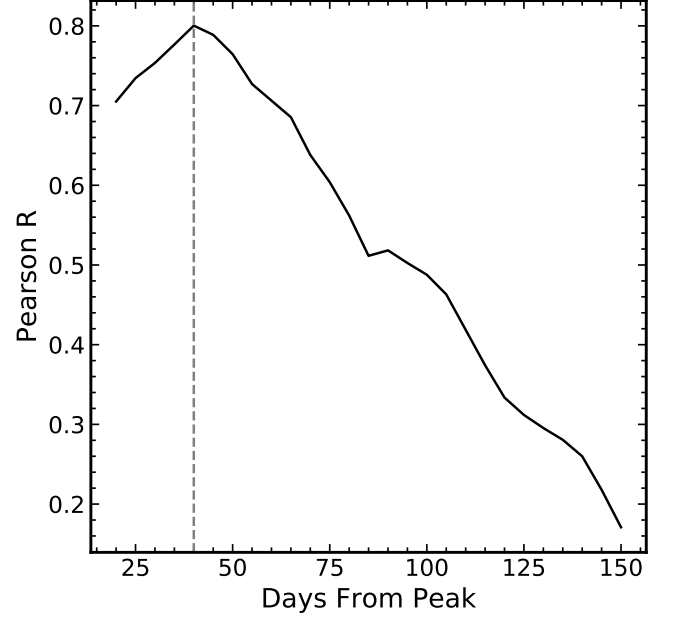


**Figure 2.** Pearson R correlation coefficient for the relationship between  $\log_{10}(L_{\text{peak}})$  and  $\Delta L_N$  where we sampled  $N$  in steps of 5 days from 20 days after peak until 150 days after peak. The dashed gray line indicates the chosen value of 40 days at the maximum Pearson R value of 0.81.

We quantified the decline-rate of TDEs using a similar parameterization to  $\Delta M_{15}$  in the Phillips relation with

$$\Delta L_N = \log_{10} \left( \frac{L_N}{L_{\text{peak}}} \right) = \log_{10}(L_N) - \log_{10}(L_{\text{peak}}) \quad (1)$$

where  $L_N$  is the luminosity of the TDE at  $N$  days after peak. We calculated  $\Delta L_N$  by fitting a line to the data within 10 days of  $N$ , centered on  $N$ , and taking the intercept minus the peak luminosity. For the class “C” objects, we added the uncertainty on the intercept in quadrature with uncertainty on the peak luminosity to estimate the error in  $\Delta L_N$ . To determine the optimal  $N$  at which to measure the decline-rate, we computed the Pearson R correlation coefficient between  $L_{\text{peak}}$  and  $\Delta L_N$  for  $20 < N < 150$  in 5 day steps. A Pearson R value near 1 or  $-1$  indicates perfect correlation or negative correlation, respectively, whereas a value near 0 implies no correlation. As seen in Figure 2, the highest Pearson R is 0.81 at 40 days. For the rest of the study we adopt  $N = 40$  days, although this may need to be modified as more TDEs are analyzed.

The resulting correlation between  $L_{\text{peak}}$  and  $\Delta L_{40}$  is shown in Figure 3. If we fit this with a linear function, the best fit is

$$\log_{10}(L_{\text{peak}} / (\text{erg s}^{-1})) = (44.1^{+0.1}_{-0.1}) + (1.1^{+0.3}_{-0.3})(\Delta L_{40} + 0.5) \quad (2)$$

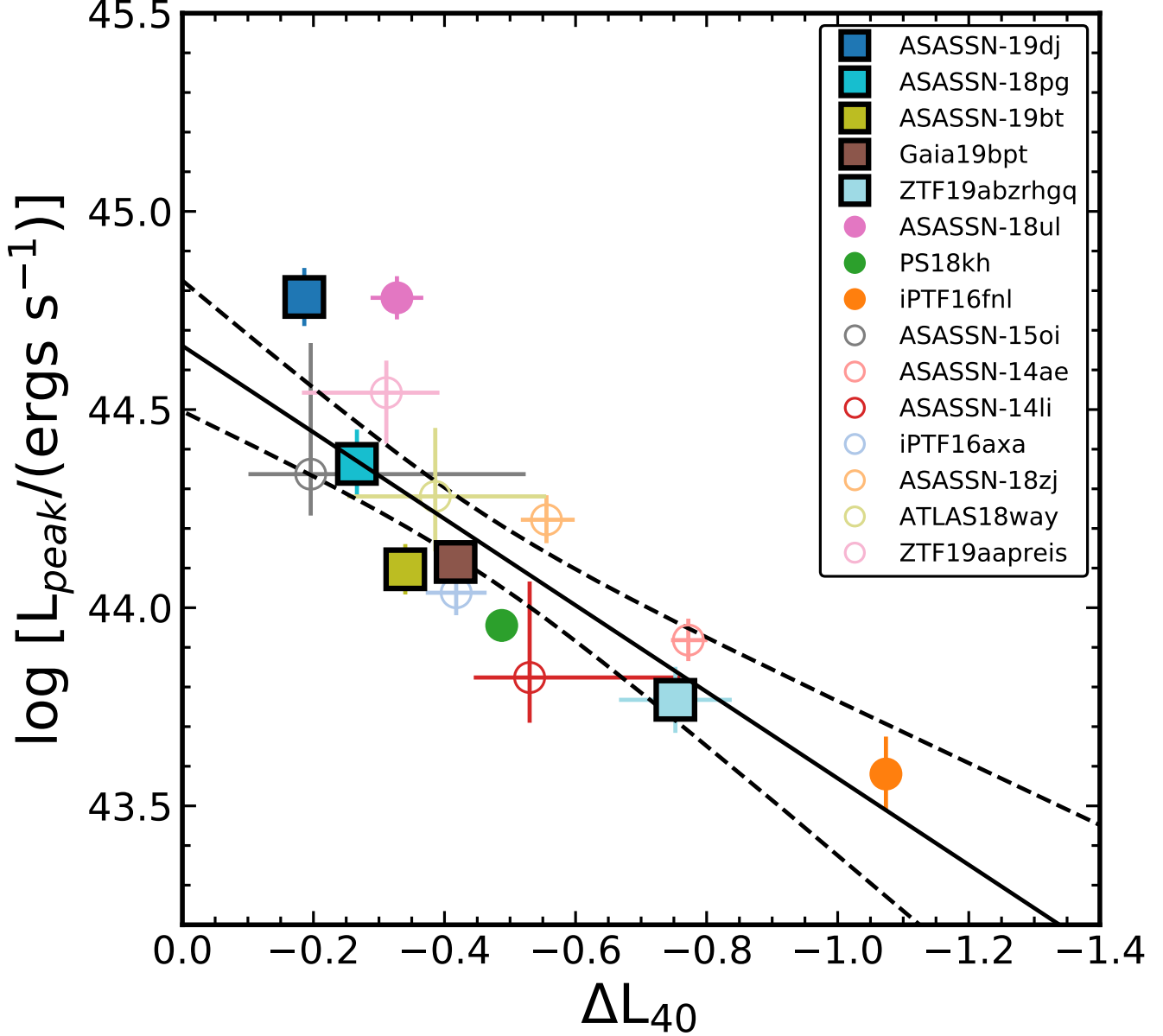


**Figure 3.** Peak bolometric UV/optical luminosity as compared to the decline rate.  $\Delta L_{40}$  is defined as  $\log_{10}(L_{40}/L_{\text{peak}})$ , where  $L_{40}$  is the luminosity of the TDE at 40 days after peak. The objects and colors are the same as in Figure 1. Filled squares with a black border are our “A” sample for which we have *Swift* data prior to the peak bolometric luminosity. Filled circles are the “B” TDEs, which have observations at longer wavelengths that constrain the bolometric peak, but lack UV observations from *Swift* to accurately fit the luminosity, and open circles are the “C” TDEs for which we could not constrain the bolometric peak. The solid black line is the line of best fit and the dashed black lines are plus/minus one sigma from the best fit line.

where  $-0.5$  is approximately the mean of the values of  $\Delta L_{40}$ . We include the mean in the linear fits because it makes the uncertainties in the two parameters essentially uncorrelated. This is the fit using all three classes. If we fit only the Class “A” and “B” sources we find

$$\log_{10}(L_{\text{peak}}/(\text{erg s}^{-1})) = (44.1^{+0.1}_{-0.1}) + (1.2^{+0.4}_{-0.4})(\Delta L_{40} + 0.5) \quad (3)$$

which is consistent with the fit to all of the sources. The reduced  $\chi^2$  values of the two fits are 4.5 and 4.4, respectively, indicating that there is likely some intrinsic scatter. The uncertainties we quote on our best-fit parameters are the raw errors before accounting for this scatter. To estimate the intrinsic scatter, we expanded the uncertainties in  $L_{\text{peak}}$  by  $\sigma_p^2 \rightarrow \sigma_p^2 + \sigma^2$  and found that  $\sigma \simeq 0.19$  dex was needed to make the reduced  $\chi^2$



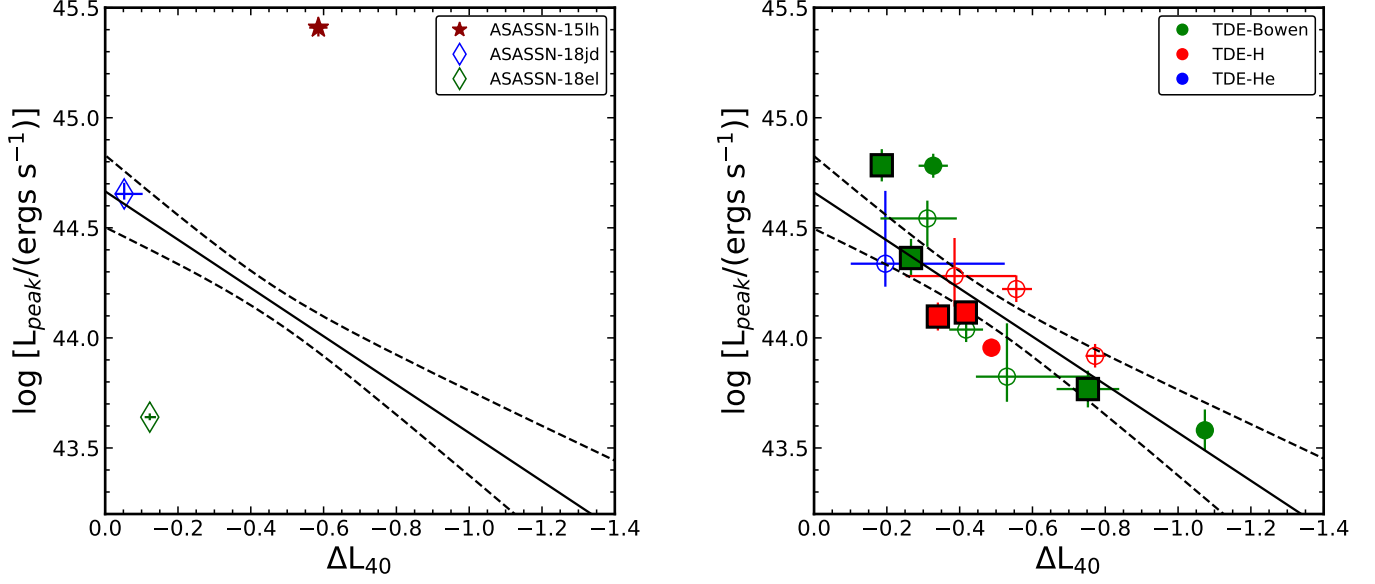


**Figure 4.** Left Panel: Other nuclear transients compared to the best-fit relationship from Figure 3. The other nuclear transients are ASASSN-15lh (a SLSN or TDE; red star), ASASSN-18jd (an AGN or TDE; blue diamond), and ASASSN-18el (a changing-look AGN; green diamond). Right Panel: TDEs from Figure 3 color-coded with respect to their spectral types (van Velzen et al. 2020). Green objects are TDE-Bowen, red are TDE-H, and blue is TDE-He.

unity. While this relationship is analogous to that seen for SNe Ia (Phillips 1993), the scatter is larger than that of the Type Ia supernovae (e.g., Folatelli et al. 2010). Given their rarity, similar peak optical magnitudes, and larger scatter, TDEs are unlikely to be competitive distance indicators.

We can gain some insight into the physical meaning of this relation by examining the scaling under the assumption that the mass of the black hole is the dominant driver of luminosities and timescales. The change in luminosity over time  $\Delta t$  is of order  $\delta L = \Delta t (L_{\text{peak}}/t_d)$ , where  $t_d$  is some decay timescale. This means that  $\Delta L_N = \log_{10}(\Delta t_N/t_d)$ , so the scaling relation in Equation 2 is that  $L_{\text{peak}} \propto t_d^{-a}$  where  $a$  is the slope of the relation. If  $t_d$  is related to the standard fall back time,  $t_d \propto t_{fb} \propto M_{BH}^{1/2}$ , then the peak luminosity scales with mass as  $L_{\text{peak}} \propto M_{BH}^{-a/2} \propto M_{BH}^{-0.55 \pm 0.15}$  given our parameters. This almost exactly matches estimates that the peak accretion rate relative to Eddington is  $\propto M_{BH}^{-3/2}$  or  $\dot{M}_{\text{peak}} \propto M_{BH}^{-1/2}$  with  $L_{\text{peak}} \propto \dot{M}_{\text{peak}}$  (e.g., Metzger & Stone 2016; Kochanek 2016b; Ryu et al. 2020).

#### 4. SUMMARY

From the TDE blackbody fits shown in Figure 1 we find the following trends:

- The blackbody radii generally are largest near peak and monotonically decline as time passes. At late times ( $\gtrsim 200$  days), the blackbody radius con-

tinues to decrease slowly. The TDE-Bowen objects generally have smaller effective blackbody radii than the TDE-H objects.

- Most of the TDEs have roughly constant temperatures with some small-scale variations. Only a handful of objects show large-scale increases or decreases in their temperature. The TDE-Bowen objects are generally hotter than the TDE-H objects.
- The luminosities of the TDEs generally evolve smoothly, but some exhibit multiple spikes in luminosity. At late times, the luminosities of the TDEs flatten out.
- As can be seen in Figure 1, more luminous TDEs fade more slowly. The correlation is strongest when we use the decline over 40 days, with a slope of  $\log_{10}(L_{\text{peak}}) \sim (1.1^{+0.3}_{-0.3})(\Delta L_{40} + 0.5)$ .

There seem to be few trends between the spectral type of a TDE (van Velzen et al. 2020) and its position on the peak-luminosity/decline-rate diagram. Both the most and least luminous sources are TDE-Bowen objects, with the TDE-H objects falling in between. Accordingly, neither spectral type of TDE appears to decay faster than the other. The TDE-Bowen objects appear to have slightly larger scatter about the correlation.

The correlation between peak luminosity and decline rate may also provide a diagnostic for whether sources are actually TDEs. Figure 4 shows the correlation found

for TDEs along with several other nuclear transients. ASASSN-18el (Trakhtenbrot et al. 2019) is a changing look AGN with no present arguments in favor of it being a TDE, and we see that it lies far off the relation. ASASSN-18jd shows similarities to both TDEs and nuclear flares that look different from normal AGN variability (Neustadt et al. 2019), but here we see that it lies on the relation, albeit with the caveat that it is a class “C” source. Dong et al. (2016) and Bersten et al. (2016) classify ASASSN-15lh as a Type I superluminous supernova (SLSN), while Leloudas et al. (2016) classify it as a TDE, even though no well-studied TDEs show similar spectroscopic properties or evolution. Here we see that it lies far off the correlation, supporting the SLSN classification.

The biggest shortcoming of the present sample is that roughly half of the sources were not observed at peak (the class “C” sources). This is a further reason to emphasize the early discovery and classification of TDEs, which fortunately seems to be increasingly common due to a growing number of transient surveys covering large fractions of the sky at high cadence and with significant survey overlaps. To further test this correlation observationally, it will be necessary to discover more TDEs early in their evolution and obtain high signal-to-noise ratio *Swift* UVOT follow-up photometry, as accurately fitting the blackbody components of TDEs requires UV coverage. If follow-up of future TDEs confirms this correlation, theoretical simulations and models of the UV and optical emission from TDEs must be able explain this trend.

## ACKNOWLEDGMENTS

We thank Michael Tucker and Aaron Do for helpful comments on the manuscript and Gagandeep Anand for useful discussions that improved our error analysis. We thank Jack Neustadt for sharing blackbody fits for ASASSN-18jd.

We thank the Las Cumbres Observatory and its staff for its continuing support of the ASAS-SN project. ASAS-SN is supported by the Gordon and Betty Moore Foundation through grant GBMF5490 to the Ohio State University, and NSF grants AST-1515927 and AST-1908570. Development of ASAS-SN has been supported by NSF grant AST-0908816, the Mt. Cuba Astronomical Foundation, the Center for Cosmology and AstroParticle Physics at the Ohio State University, the Chinese Academy of Sciences South America Center for Astronomy (CAS- SACA), the Villum Foundation, and George Skestos.

BJS, KZS, and CSK are supported by NSF grants AST-1515927, AST-1814440, and AST-1908570. BJS is also supported by NSF grants AST-1920392 and AST-1911074. KAA is supported by the Danish National Research Foundation (DNRF132). TAT is supported in part by NASA grant 80NSSC20K0531. Support for JLP is provided in part by FONDECYT through the grant 1191038 and by the Ministry of Economy, Development, and Tourism’s Millennium Science Initiative through grant IC120009, awarded to The Millennium Institute of Astrophysics, MAS.

*Facilities:* ASAS-SN, Swift(UVOT)

*Software:* emcee (Foreman-Mackey et al. 2013)

## REFERENCES

- Bellm, E. C., Kulkarni, S. R., Graham, M. J., et al. 2019, *PASP*, 131, 018002, doi: [10.1088/1538-3873/aaeabe](https://doi.org/10.1088/1538-3873/aaeabe)
- Bersten, M. C., Benvenuto, O. G., Orellana, M., & Nomoto, K. 2016, *ApJL*, 817, L8, doi: [10.3847/2041-8205/817/1/L8](https://doi.org/10.3847/2041-8205/817/1/L8)
- Brown, J. S., Shappee, B. J., Holoiien, T. W.-S., et al. 2016, *MNRAS*, 462, 3993, doi: [10.1093/mnras/stw1928](https://doi.org/10.1093/mnras/stw1928)
- Brown, J. S., Kochanek, C. S., Holoiien, T. W.-S., et al. 2018, *MNRAS*, 473, 1130, doi: [10.1093/mnras/stx2372](https://doi.org/10.1093/mnras/stx2372)
- Chambers, K. C., Magnier, E. A., Metcalfe, N., et al. 2016, *ArXiv e-prints*. <https://arxiv.org/abs/1612.05560>
- Coughlin, E. R., & Nixon, C. J. 2019, *ApJL*, 883, L17, doi: [10.3847/2041-8213/ab412d](https://doi.org/10.3847/2041-8213/ab412d)
- Dai, L., McKinney, J. C., Roth, N., Ramirez-Ruiz, E., & Miller, M. C. 2018, *ApJL*, 859, L20, doi: [10.3847/2041-8213/aab429](https://doi.org/10.3847/2041-8213/aab429)
- Dong, S., Bose, S., Chen, P., et al. 2018, *The Astronomer’s Telegram*, 12198, 1
- Dong, S., Shappee, B. J., Prieto, J. L., et al. 2016, *Science*, 351, 257. <https://arxiv.org/abs/1507.03010>
- Evans, C. R., & Kochanek, C. S. 1989, *ApJL*, 346, L13, doi: [10.1086/185567](https://doi.org/10.1086/185567)
- Folatelli, G., Phillips, M. M., Burns, C. R., et al. 2010, *AJ*, 139, 120, doi: [10.1088/0004-6256/139/1/120](https://doi.org/10.1088/0004-6256/139/1/120)
- Foreman-Mackey, D., Hogg, D. W., Lang, D., & Goodman, J. 2013, *PASP*, 125, 306, doi: [10.1086/670067](https://doi.org/10.1086/670067)



- Freedman, W. L., Madore, B. F., Hatt, D., et al. 2019, *ApJ*, 882, 34, doi: [10.3847/1538-4357/ab2f73](https://doi.org/10.3847/1538-4357/ab2f73)
- Gallegos-Garcia, M., Law-Smith, J., & Ramirez-Ruiz, E. 2018, *ApJ*, 857, 109, doi: [10.3847/1538-4357/aab5b8](https://doi.org/10.3847/1538-4357/aab5b8)
- Gehrels, N., Chincarini, G., Giommi, P., et al. 2004, *ApJ*, 611, 1005, doi: [10.1086/422091](https://doi.org/10.1086/422091)
- Gezari, S., Cenko, S. B., & Arcavi, I. 2017, *ApJL*, 851, L47, doi: [10.3847/2041-8213/aaa0c2](https://doi.org/10.3847/2041-8213/aaa0c2)
- Gezari, S., van Velzen, S., Perley, D. A., et al. 2019, *The Astronomer's Telegram*, 12789, 1
- Golightly, E. C. A., Coughlin, E. R., & Nixon, C. J. 2019, *ApJ*, 872, 163, doi: [10.3847/1538-4357/aafd2f](https://doi.org/10.3847/1538-4357/aafd2f)
- Graham, A. W., Erwin, P., Caon, N., & Trujillo, I. 2001, *ApJL*, 563, L11, doi: [10.1086/338500](https://doi.org/10.1086/338500)
- Guillochon, J., & Ramirez-Ruiz, E. 2013, *ApJ*, 767, 25, doi: [10.1088/0004-637X/767/1/25](https://doi.org/10.1088/0004-637X/767/1/25)
- . 2015, *ApJ*, 809, 166, doi: [10.1088/0004-637X/809/2/166](https://doi.org/10.1088/0004-637X/809/2/166)
- Holoien, T. W.-S., Brown, J. S., Auchettl, K., et al. 2018, *MNRAS*, 480, 5689, doi: [10.1093/mnras/sty2273](https://doi.org/10.1093/mnras/sty2273)
- Holoien, T. W.-S., Prieto, J. L., Bersier, D., et al. 2014, *MNRAS*, 445, 3263, doi: [10.1093/mnras/stu1922](https://doi.org/10.1093/mnras/stu1922)
- Holoien, T. W.-S., Kochanek, C. S., Prieto, J. L., et al. 2016a, *MNRAS*, 455, 2918, doi: [10.1093/mnras/stv2486](https://doi.org/10.1093/mnras/stv2486)
- . 2016b, *MNRAS*, 463, 3813, doi: [10.1093/mnras/stw2272](https://doi.org/10.1093/mnras/stw2272)
- Holoien, T. W. S., Vallely, P. J., Auchettl, K., et al. 2019a, *ApJ*, 883, 111, doi: [10.3847/1538-4357/ab3c66](https://doi.org/10.3847/1538-4357/ab3c66)
- Holoien, T. W. S., Huber, M. E., Shappee, B. J., et al. 2019b, *ApJ*, 880, 120, doi: [10.3847/1538-4357/ab2ae1](https://doi.org/10.3847/1538-4357/ab2ae1)
- Hung, T., Gezari, S., Blagorodnova, N., et al. 2017, *ApJ*, 842, 29, doi: [10.3847/1538-4357/aa7337](https://doi.org/10.3847/1538-4357/aa7337)
- Kochanek, C. S. 1994, *ApJ*, 422, 508, doi: [10.1086/173745](https://doi.org/10.1086/173745)
- . 2016a, *MNRAS*, 458, 127, doi: [10.1093/mnras/stw267](https://doi.org/10.1093/mnras/stw267)
- . 2016b, *MNRAS*, 461, 371, doi: [10.1093/mnras/stw1290](https://doi.org/10.1093/mnras/stw1290)
- Kochanek, C. S., Shappee, B. J., Stanek, K. Z., et al. 2017, *PASP*, 129, 104502, doi: [10.1088/1538-3873/aa80d9](https://doi.org/10.1088/1538-3873/aa80d9)
- Lacy, J. H., Townes, C. H., & Hollenbach, D. J. 1982, *ApJ*, 262, 120, doi: [10.1086/160402](https://doi.org/10.1086/160402)
- Leloudas, G., Fraser, M., Stone, N. C., et al. 2016, *Nature Astronomy*, 1, 0002, doi: [10.1038/s41550-016-0002](https://doi.org/10.1038/s41550-016-0002)
- Leloudas, G., Dai, L., Arcavi, I., et al. 2019, *arXiv e-prints*. <https://arxiv.org/abs/1903.03120>
- Liu, X.-L., Dou, L.-M., Shen, R.-F., & Chen, J.-H. 2019, *arXiv e-prints*, *arXiv:1912.06081*. <https://arxiv.org/abs/1912.06081>
- Lu, W., & Bonnerot, C. 2019, *MNRAS*, 3033, doi: [10.1093/mnras/stz3405](https://doi.org/10.1093/mnras/stz3405)
- MacLeod, C. L., Ivezić, Ž., Sesar, B., et al. 2012, *ApJ*, 753, 106, doi: [10.1088/0004-637X/753/2/106](https://doi.org/10.1088/0004-637X/753/2/106)
- Metzger, B. D., & Stone, N. C. 2016, *MNRAS*, 461, 948, doi: [10.1093/mnras/stw1394](https://doi.org/10.1093/mnras/stw1394)
- Mockler, B., Guillochon, J., & Ramirez-Ruiz, E. 2019, *ApJ*, 872, 151, doi: [10.3847/1538-4357/ab010f](https://doi.org/10.3847/1538-4357/ab010f)
- Neustadt, J. M. M., Holoien, T. W. S., Kochanek, C. S., et al. 2019, *arXiv e-prints*, *arXiv:1910.01142*. <https://arxiv.org/abs/1910.01142>
- Phillips, M. M. 1993, *ApJL*, 413, L105, doi: [10.1086/186970](https://doi.org/10.1086/186970)
- Phinney, E. S. 1989, *Nature*, 340, 595, doi: [10.1038/340595a0](https://doi.org/10.1038/340595a0)
- Poole, T. S., Breeveld, A. A., Page, M. J., et al. 2008, *MNRAS*, 383, 627, doi: [10.1111/j.1365-2966.2007.12563.x](https://doi.org/10.1111/j.1365-2966.2007.12563.x)
- Rees, M. J. 1988, *Nature*, 333, 523, doi: [10.1038/333523a0](https://doi.org/10.1038/333523a0)
- Roming, P. W. A., Kennedy, T. E., Mason, K. O., et al. 2005, *SSR*, 120, 95, doi: [10.1007/s11214-005-5095-4](https://doi.org/10.1007/s11214-005-5095-4)
- Ryu, T., Krolik, J., Piran, T., & Noble, S. C. 2020, *arXiv e-prints*, *arXiv:2001.03501*. <https://arxiv.org/abs/2001.03501>
- Shappee, B. J., Prieto, J. L., Grupe, D., et al. 2014, *ApJ*, 788, 48, doi: [10.1088/0004-637X/788/1/48](https://doi.org/10.1088/0004-637X/788/1/48)
- Tonry, J. L., Denneau, L., Heinze, A. N., et al. 2018, *PASP*, 130, 064505, doi: [10.1088/1538-3873/aabadf](https://doi.org/10.1088/1538-3873/aabadf)
- Trakhtenbrot, B., Arcavi, I., MacLeod, C. L., et al. 2019, *ApJ*, 883, 94, doi: [10.3847/1538-4357/ab39e4](https://doi.org/10.3847/1538-4357/ab39e4)
- Tully, R. B., Courtois, H. M., & Sorce, J. G. 2016, *AJ*, 152, 50, doi: [10.3847/0004-6256/152/2/50](https://doi.org/10.3847/0004-6256/152/2/50)
- Ulmer, A. 1999, *ApJ*, 514, 180, doi: [10.1086/306909](https://doi.org/10.1086/306909)
- van Velzen, S., & Farrar, G. R. 2014, *ApJ*, 792, 53, doi: [10.1088/0004-637X/792/1/53](https://doi.org/10.1088/0004-637X/792/1/53)
- van Velzen, S., Gezari, S., Cenko, S. B., et al. 2018, *The Astronomer's Telegram*, 12263, 1
- van Velzen, S., Gezari, S., Hammerstein, E., et al. 2020, *arXiv e-prints*, *arXiv:2001.01409*. <https://arxiv.org/abs/2001.01409>
- Wevers, T., Pasham, D. R., van Velzen, S., et al. 2019, *MNRAS*, 488, 4816, doi: [10.1093/mnras/stz1976](https://doi.org/10.1093/mnras/stz1976)